Available online at www.sciencedirect.com
ScienceDirect
Trans. Nonferrous Met. Soc. China 34(2024) 392−407
Transactions of Nonferrous Metals Society of China
www.tnmsc.cn

Influence of retrogression temperature and time on microstructure, mechanical properties and corrosion behaviors of cryogenically-deformed 7A85 aluminum alloy

Dang WANG[1,2], Wen-xue ZHANG[1,3], You-ping YI[1,2,4], Shi-quan HUANG[1,2,4], Hai-lin HE[1,2], Jing-jing ZHANG[2,4]

1. Research Institute of Light Alloy, Central South University, Changsha 410083, China;
2. State Key Laboratory of High Performance Complex Manufacturing, Changsha 410083, China;
3. Capital Aerospace Machinery Corporation Limited, Beijing 100076, China;
4. School of Mechanical and Electrical Engineering, Central South University, Changsha 410083, China

Received 19 June 2022; accepted 24 November 2022

Abstract: To balance the strength, plasticity, and corrosion resistance of the alloy, the microstructure and comprehensive properties of cryogenically-deformed 7A85 aluminum alloy at various retrogression temperatures and time were investigated. The results showed that under the retrogression and re-aging (RRA) of lower retrogression temperature and time and T6 (120 °C, 24 h) tempers, the alloy had higher strength but poorer corrosion resistance. For RRA, increasing the retrogression temperature and time within a certain range reduced the strength but significantly improved the electrical conductivity and corrosion resistance of the alloy. However, excessively increasing the retrogression temperature and time led to a reduction in corrosion resistance. At the same retrogression temperature, the elongation of the alloy first decreased and then increased with the extension of retrogression time. The optimal temper matched to the three-dimensional cryogenically deformed 7A85 aluminum alloy was RRA180-0.5 ((120 °C, 24 h) + (180 °C, 0.5 h) + (120 °C, 24 h)).

Key words: cryogenically-deformed 7A85 aluminum alloy; retrogression temperature; retrogression time; strength; corrosion resistance; optimal temper

1 Introduction

Owing to their light weight, high strength, toughness, fatigue resistance, and damage tolerance, 7xxx series aluminum alloys are widely used in the aerospace industry [1−4]. However, they are sensitive to corrosion such as intergranular and exfoliation corrosions and suffer from conflicting strength, toughness, and corrosion resistance [5,6], which seriously restricts their further development. As typical age-strengthened alloys, the precipitate regulation during aging treatments plays an irreplaceable role in the balance of various performances of 7xxx series aluminum alloys [7−9]. Compared with single-stage (T6) and double aging treatments, the retrogression and re-aging (RRA) treatment is more likely to balance the strength and corrosion resistance of the alloy [10,11]. Based on this, numerous studies have been conducted by many scholars.

ZHONG et al [12] performed RRA treatment on a Zr + Er modified Al−Zn−Mg−Cu alloy and found that uniformly diffused matrix precipitates and a narrow precipitate-free zone (PFZ) could significantly improve the strength of the alloy. In addition, coarse grain boundary precipitates (GBPs) with wider PFZs were found to be beneficial to

Corresponding author: Wen-xue ZHANG, Tel: +86-18610630540, Fax: +86-731-88830294, E-mail: titanszhang@126.com;
You-ping YI, Tel: +86-18874869619, Fax: +86-731-88830294, E-mail: yyp@csu.edu.cn
DOI: 10.1016/S1003-6326(23)66406-4

enhancing the corrosion resistance. WANG et al [13] revealed that the best RRA aging temper for 7085 aluminum alloy was 120 °C for 24 h, 160 °C for 1.5 h, and 120 °C for 24 h, which increased the hardness by 10.2% compared to the T6 (120 °C for 24 h) temper. The improved corrosion resistance of this temper was attributed to the higher Cu content of the coarse η phase at the grain boundaries and the PFZ with a width of 45−50 nm. In addition, LI et al [14] retrogressed an AA7150 aluminum alloy at the retrogression temperatures of 175, 185, and 195 °C for 0.25−3 h. They found that a retrogression time less than 3 h may achieve a strength higher than that of peak-aged T6, with the best combination of corrosion resistance and strength acquired at a retrogression temper of 175 °C for 3 h. Similarly, OZER and KARAASLAN [15] applied the retrogression processes of 180, 240, and 320 °C for 1, 30, 50, 70, 90, and 120 min to AA7075 aluminum alloy. The results showed that the retrogression temperatures and time influenced the hardness, toughness, and electrical conductivity of the alloy by regulating the precipitates. The impact toughness was inversely related to the hardness, with the highest impact toughness and lowest strength observed at a retrogression of 320 °C for 120 min.

Most of these studies only regulated the precipitates during heat treatment, and the combination of cryogenic deformation and retrogression treatment was rarely reported. Moreover, the effect of PFZ on corrosion resistance is controversial. To reduce the adverse effects of the coarse second-phase particles on the properties of the alloy, the 7A85 aluminum alloy was subjected to three-dimensional cryogenic deformation in this study to crush coarse particles and dissolve them in subsequent solution treatment. The effects of various retrogression temperatures and time on the microstructure, electrical conductivity, mechanical properties, and corrosion resistance of the alloy were studied. Finally, the optimal retrogression temper matching the three-dimensional cryogenic deformation was obtained, and the relationship between the microstructure and properties of the alloy was discussed in detail.

2 Experimental

2.1 Materials and heat treatments

The as-cast 7A85 aluminum alloy (Al, 7.0−8.0 Zn, 1.2−1.8 Mg, 1.3−2.0 Cu, 0.08−0.15 Zr, ~0.08 Fe, and ~0.06 Si, in wt.%) in this study was prepared by the Central South University of China. A rectangular sample with dimensions of 140 mm × 130 mm × 210 mm was cut from a large homogenized ingot (460 °C for 12 h). Multi-directional forging using a seven-upsetting and six-cross-stretching method was then performed on the sample (57% deformation at 470 °C, further details in a separate paper [16]). To reduce the adverse effects of coarse second-phase particles on the alloy properties, the forging sample was subjected to three-dimensional cryogenic deformation with a 20% height reduction per direction. Prior to this, the material underwent an annealing process at 400 °C for 2 h to eliminate internal defects to prevent fractures during cryogenic deformation. The large cryogenically-deformed sample was cut into smaller pieces as the initial specimen for the current heat treatment study.

Figure 1 shows the sample preparation route and heat treatment process. The heat treatment of the cryogenically-deformed specimens included the solution treatment (480 °C for 6 h), water quenching, and single-stage or RRA aging treatments. The conventional single-stage aging treatment was T6 (120 °C for 24 h), while the RRA aging treatment involved pre-aging at 120 °C for 24 h, retrogression at 160−190 °C for 0.25−8 h, and re-aging at 120 °C for 24 h. The detailed aging tempers are shown in Table 1. All retrogressed specimens were quenched in water to increase the precipitation force during the subsequent re-aging process.

2.2 Tensile and corrosion tests

The tensile samples used to test the mechanical

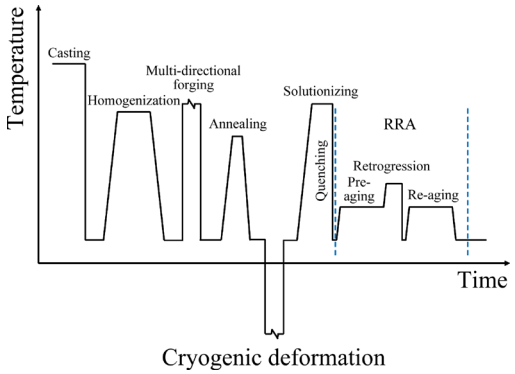

Fig. 1 Sample preparation route and heat treatment process

Table 1 Details of T6 and RRA aging tempers

Temper code	Aging treatment		
	Pre-aging	Retrogression	Re-aging
T6	120 °C, 24 h		
RRA160	120 °C, 24 h	160 °C, 1, 2, 4, 8 h	120 °C, 24 h
RRA170	120 °C, 24 h	170 °C, 1, 2, 4, 6, 8 h	120 °C, 24 h
RRA180	120 °C, 24 h	180 °C, 0.25, 0.5, 1, 2, 4, 6 h	120 °C, 24 h
RRA190	120 °C, 24 h	190 °C, 0.5, 1, 2, 4, 6 h	120 °C, 24 h

properties of each alloy were cut from the aged specimens along the same height direction as the original thick plate ingot, whose dimensions conformed to the GB/T 228—2002 standard (Fig. 2). The tensile tests were performed on an electronic universal testing machine (WDW−100A) with a tensile rate of 1.68 mm/min (by a strain rate conversion of 0.01 s^{-1}), and the tensile samples for tensile test were not corroded. The electrical conductivity was measured with a D60K digital metal conductivity meter based on the ASTM E1004 standard.

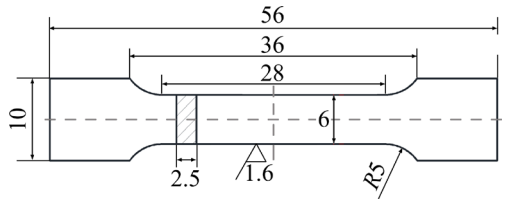

Fig. 2 Dimensions of tensile specimens (Unit: mm)

The intergranular corrosion tests were carried out according to the GB/T 7998—2005 standard. The specimens were wiped with ethanol and then immersed in sodium hydroxide solution for 5−15 min. After removal, they were washed with deionized water and immersed in nitric acid solution until the surface was clean. Finally, the specimens were washed again with deionized water and suspended in corrosion solution (57 g NaCl + 1 L H_2O + 10 mL H_2O_2) at (35±2) °C for 6 h. The corrosion depth was measured using an optical microscope, and the maximum value was used as the basis for judging the intergranular corrosion performance. The exfoliation corrosion tests were conducted in accordance with the GB/T 22639—2008 standard, wherein cleaned specimens were immersed in corrosion solution (234 g NaCl + 50 g KNO_3 + 1 L H_2O + 6.3 mL HNO_3) at (25±3) °C for 48 h. After impregnation, they were rated for exfoliation corrosion based on their surface morphologies under wet conditions.

2.3 Microstructure observation

The microstructures were observed through the central parts of the specimens in the same length–height (*L*−*H*) plane as the original thick plate ingot. Scanning electron microscopy (SEM; TESCAN MIRA3 LUM) was used to describe the fracture surface morphology, while transmission electron microscopy (TEM; FEI Titan G2 60−300) was employed to characterize the matrix precipitates and GBPs of the alloy after various aging treatments. The TEM specimens were prepared by first being ground to a thickness of 80−100 μm and then thinned in an electrolyte (30% HNO_3 + 70% CH_3OH) at −25 °C via a twin-jet electropolisher. The current was set to be 60 mA.

3 Results

3.1 Mechanical properties and electrical conductivity

Figure 3 shows the mechanical properties and electrical conductivity of 7A85 aluminum alloy under various aging treatments. The mechanical properties include the ultimate tensile strength (UTS), yield strength (YS), and elongation (EL). The change patterns of the UTS and YS were observed to be synchronized under different RRA aging tempers (Figs. 3(a) and (b)). The increase in retrogression temperature and time resulted in a decrease in the UTS and YS, except for RRA160 which increased first and then decreased upon extending the aging time. Furthermore, the UTS and YS decreased more rapidly with increasing retrogression time at a higher retrogression temperature. An UTS comparable to that of the T6 state could only be achieved at a lower retrogression

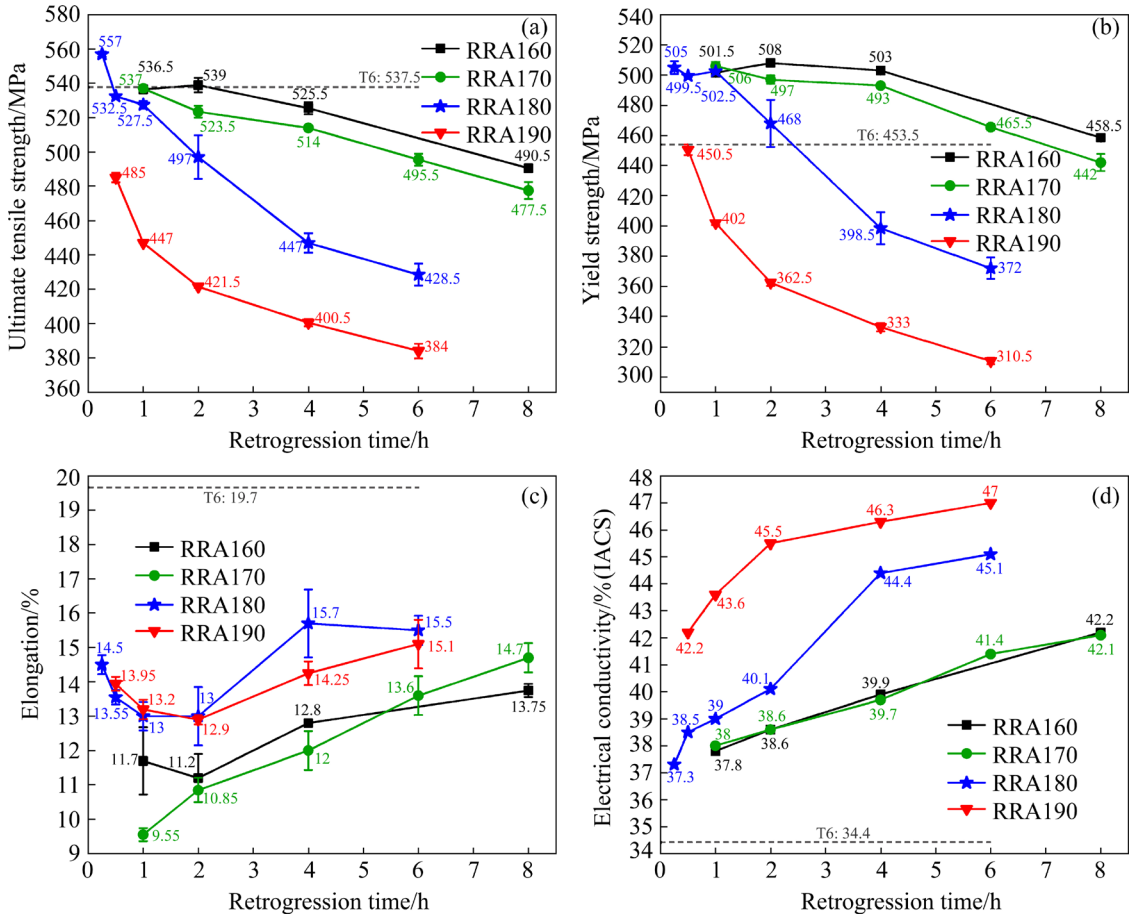

Fig. 3 Mechanical properties and electrical conductivity of 7A85 aluminum alloy after T6 and various RRA treatments: (a) Ultimate tensile strength; (b) Yield strength; (c) Elongation; (d) Electrical conductivity

temperature and time, exceeding that of the T6 state at a suitable retrogression temperature with a very short retrogression time (e.g., RRA180-0.25). Notably, the RRA aging treatment could significantly improve the low YS of T6. Figure 3(c) indicates that the EL of RRA170 increased with an extended retrogression time, while it first decreased and then increased for RRA160, RRA180, and RRA190. A high EL was more easily obtained in the RRA temper within a retrogression temperature range of 180−190 °C, although it was much lower than that of T6.

The influence of the retrogression time on the conductivity at the four retrogression temperatures followed the same pattern, i.e., increasing the retrogression temperature and time caused a significant increase in conductivity. Furthermore, when the retrogression time was prolonged, the conductivity growth rates of RRA160 and RRA170 were essentially constant, while those of RRA180 and RRA190 first increased (above the growth rates of RRA160 and RRA170) and then decreased (comparable to the growth rates of RRA160 and RRA170). Many studies have shown that high electrical conductivity was beneficial to enhancing the corrosion resistance of the alloys [13,17]. By comprehensively considering mechanical properties and electrical conductivities, the recommended retrogression temperature and time ranges were therefore 160 °C for 2−4 h, 170 °C for 1−4 h, and 180 °C for 0.25−1 h. Because of the severe strength loss of the alloy at the retrogression temperature of 190 °C and the fact that short retrogression time of 0.25 h at 190 °C is difficult to control industrially, a retrogression temper of 190 °C for 0.5 h was chosen as a control against that of 180 °C for 0.5 h in subsequent study. The following sections of corrosion and microstructure tests thus focus on these tempers.

3.2 Corrosion properties

3.2.1 Intergranular corrosion

Figure 4 represents the maximum intergranular corrosion (IGC) depths of specimens after various

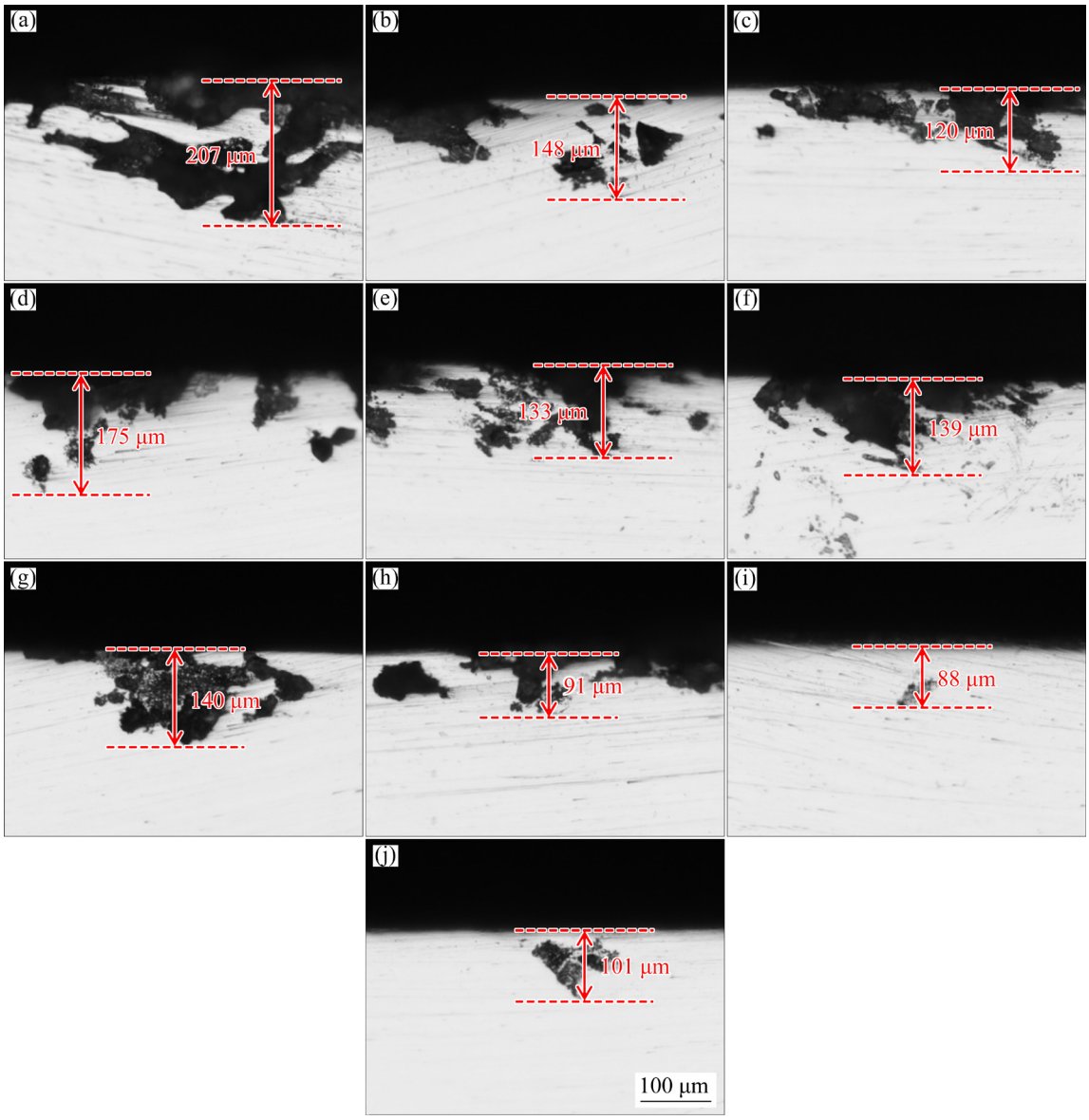

Fig. 4 Maximum intergranular corrosion depths of samples after T6 and various RRA treatments: (a) T6; (b) RRA160-2; (c) RRA160-4; (d) RRA170-1; (e) RRA170-2; (f) RRA170-4; (g) RRA180-0.25; (h) RRA180-0.5; (i) RRA180-1; (j) RRA190-0.5

aging treatments (selected from Section 3.1 with better performance). The IGC depths of T6, RRA160-2, RRA160-4, RRA170-1, RRA170-2, RRA170-4, RRA180-0.25, RRA180-0.5, RRA180-1, and RRA190-0.5 were 207, 148, 120, 175, 133, 139, 140, 91, 88, and 101 μm, respectively. It could be concluded that the IGC resistance increased in the following order: T6 < RRA170-1 < RRA160-2 < RRA180-0.25 < RRA170-4 < RRA170-2 < RRA160-4 < RRA190-0.5 < RRA180-0.5 < RRA180-1.

As can be seen from the cross-sections, the RRA tempers significantly reduced the maximum corrosion depth and improved the IGC resistance compared with the T6 temper (Fig. 4(a)). For RRA, the IGC resistance increased upon extending the retrogression time from 2 to 4 h at 160 °C (Figs. 4(b) and (c)), while it increased first and then decreased upon extending retrogression time from 1 to 4 h at 170 °C (Figs. 4(d–f)) and from 0.25 to 1 h at 180 °C (Figs. 4(g–i)). At a retrogression time of 0.5 h, the IGC resistance decreased when the retrogression temperature was increased from 180 to 190 °C. Therefore, appropriately increasing the retrogression temperature and time could improve the IGC resistance of the alloy, whereas excessively

increasing the retrogression temperature or time caused a reduction in IGC resistance. The retrogression at 180 °C for 0.5 and 1 h respectively resulted in better IGC resistances of 56% and 57.5% reductions in the maximum IGC depth compared to T6.

3.2.2 Exfoliation corrosion

The morphologies and corresponding grades of the exfoliation corrosion (EXCO) are shown in Fig. 5 and Table 2, respectively. According to the

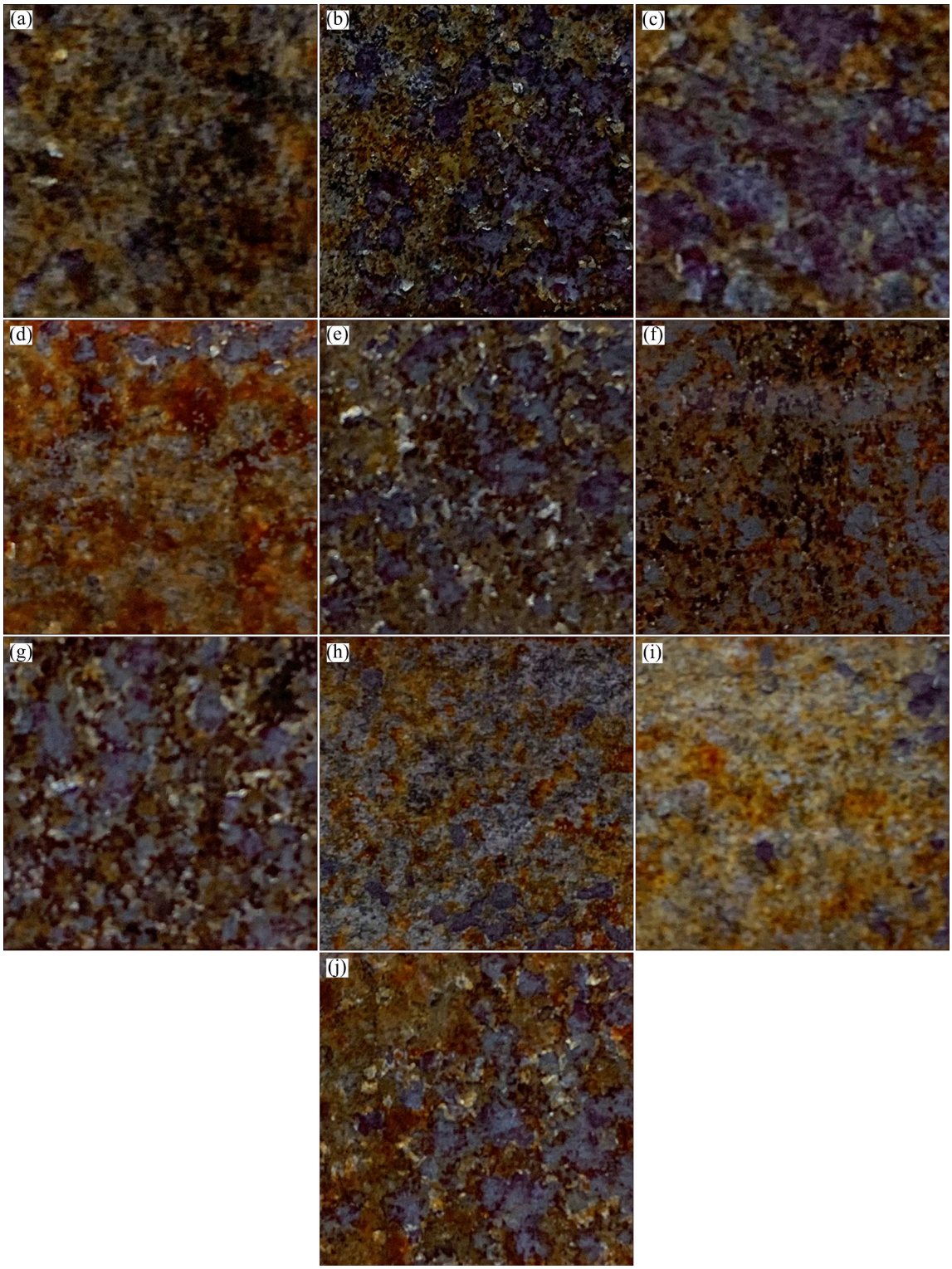

Fig. 5 Exfoliation corrosion macro-morphologies of samples after T6 and various RRA treatments: (a) T6; (b) RRA160-2; (c) RRA160-4; (d) RRA170-1; (e) RRA170-2; (f) RRA170-4; (g) RRA180-0.25; (h) RRA180-0.5; (i) RRA180-1; (j) RRA190-0.5

Table 2 Corrosion grades of 7A85-RRA aluminum alloy retrogressed at different temperatures for various time

Heat treatment	Temperature/°C	Time/h	Corrosion grade
T6	120	24	ED
RRA	160	2	ED
		4	EB
RRA	170	1	ED
		2	EB
		4	EC
RRA	180	0.25	EC
		0.5	EA
		1	P
RRA	190	0.5	EC

classification standard, the EXCO grade could be divided as follows: EA−P (light exfoliation) < EB < EC < ED (severe exfoliation). Figure 5(a) shows that the surface color of the T6 sample was the darkest after the EXCO, which revealed the most serious EXCO (ED grade). Prolonging retrogression time at 160 °C caused a lighter color of the corroded surface (reflecting increased EXCO resistance), while extending retrogression time at 170 and 180 °C resulted in an increase at first and then a decrease in the EXCO resistance. The EXCO resistance of RRA190-0.5 was lower than that of RRA180-0.5. The EXCO degrees of the T6, RRA160-2, RRA160-4, RRA170-1, RRA170-2, RRA170-4, RRA180-0.25, RRA180-0.5, RRA180-1, and RRA190-0.5 samples were ED, ED, EB, ED, EB, EC, EC, EA, P, and EC, respectively (Table 2).

The above-mentioned results demonstrated that the effect of different RRA tempers on EXCO was consistent with the IGC. Considering the resistance of the IGC and EXCO, retrogressing the alloy at 180 °C for 0.5 h or 1 h provided better corrosion resistance. However, the UTS and EL of the alloy retrogressed at 180 °C for 0.5 h were higher than those retrogressed at 180 °C for 1 h. Therefore, the comprehensive performance of the alloy was optimal in the RRA temper of (120 °C, 24 h) + (180 °C, 0.5 h) + (120 °C, 24 h), with almost no loss of UTS, a 10.1% increase in YS, an 11.9% increase in electrical conductivity, and a 56% decrease in maximum IGC depth compared to T6.

3.3 Precipitation

3.3.1 Matrix precipitation

The matrix precipitate morphologies and corresponding diffraction spots (SAED patterns) of the alloys after various aging treatments by TEM observation are shown in Figs. 6 and 7, respectively. Most of the precipitates in Fig. 6 were η' ($MgZn_2$) and η ($MgZn_2$) phases, as all diffraction spots were at the $\langle 011\rangle_{Al}$ position. The diffraction spots of the η' phase at the 1/3 and 2/3 $\{022\}_{Al}$ positions and the spots of the η phase near the strong spots of the Al matrix can be observed in Fig. 7 [18,19]. The diffraction spots at $1/2\{022\}_{Al}$ are from Al_3Zr [19].

In all RRA tempers, the matrix precipitates mainly contained needle-like η' phases of 4−13 nm in length and 1−3 nm in width as well as rod-like η phases of 4−8 nm in length and 3−5 nm in width. Some exceptions were the finer η' phases of 3−5 nm in length and 1−3 nm in width in the T6 sample and the coarser η phases of 5−12 nm in length and 3−7 nm in width in the RRA170-4, RRA180-1, and RRA190-0.5 samples. In addition, the matrix precipitates in the T6 sample were almost all η' phases, while matrix η' and η phases coexisted in the RRA samples. Increasing the retrogression temperature and time of RRA caused a decrease in η' phases accompanied by an increase in η phases, which was due to the growth of the η' phases into η phases in the matrix. Too high retrogression temperature and too long retrogression time resulted in the significant coarsening of the η phases, and the retrogression temperature had a greater influence than the retrogression time. After retrogression at 190 °C for 0.5 h, the matrix precipitates were dominated by extremely coarse η phases (Fig. 6(j)).

3.3.2 Grain boundary precipitation

The grain boundary precipitate (GBP) morphologies of 7A85 aluminum alloy after T6 and various RRA treatments are exhibited in Fig. 8. Their diffraction spots were consistent with those shown in Fig. 7. Similarly, the GBPs were coarse η phases owing to the diffraction spots at the $\langle 011\rangle_{Al}$ position. The effects of different aging treatments on grain boundary precipitation were mainly reflected in the size of the GBPs, the interparticle spacings of the GBPs, and the width of the PFZ. By observation, no significant PFZ was found for the RRA treatment samples with lower retrogression temperatures and shorter retrogression time (RRA160-2 and RRA170-1) or the T6 samples. As measured using Image-Pro software, the PFZ

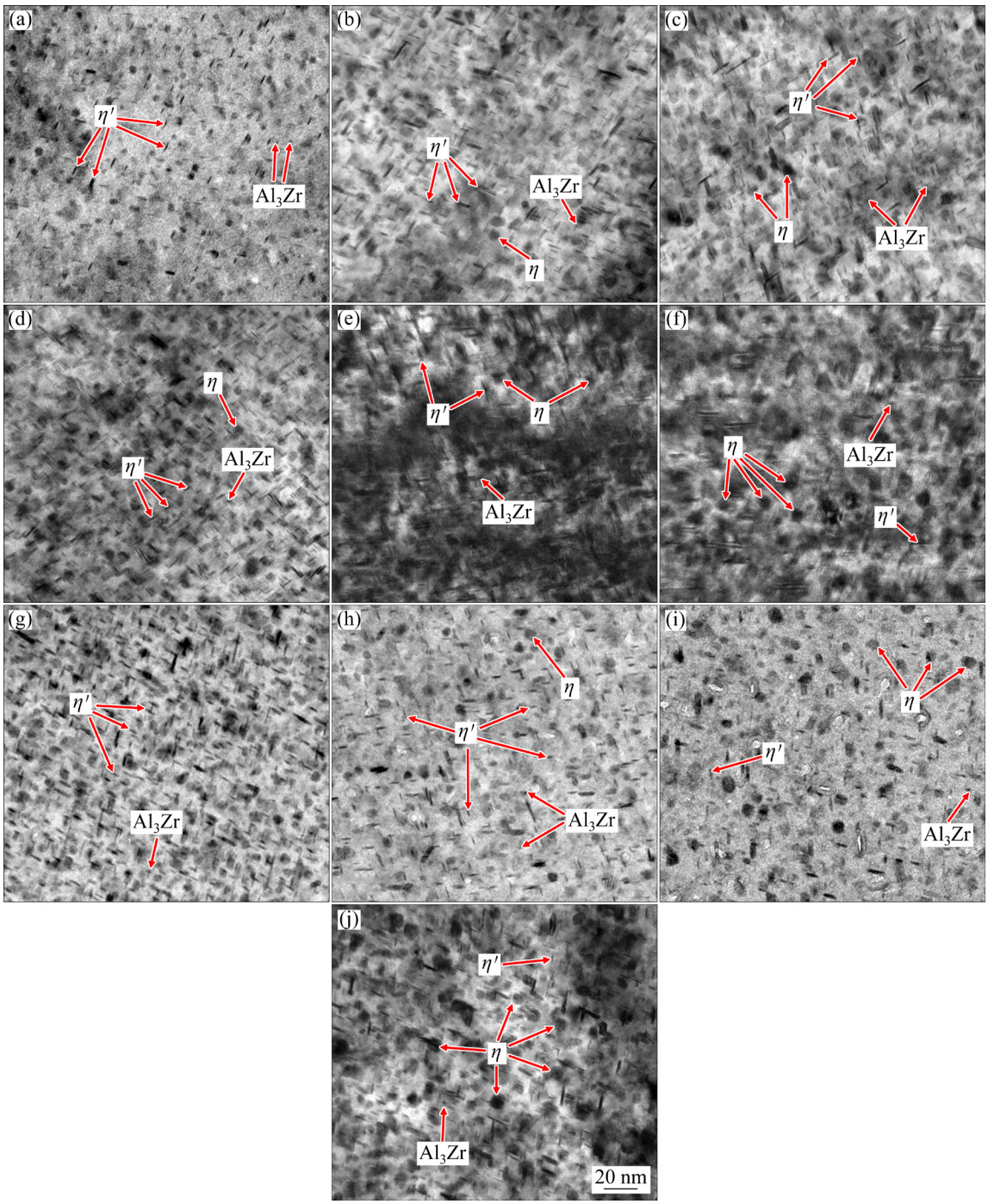

Fig. 6 Matrix precipitate morphologies of 7A85 aluminum alloy after T6 and various RRA treatments: (a) T6; (b) RRA160-2; (c) RRA160-4; (d) RRA170-1; (e) RRA170-2; (f) RRA170-4; (g) RRA180-0.25; (h) RRA180-0.5; (i) RRA180-1; (j) RRA190-0.5

widths of RRA160-4, RRA170-2, RRA170-4, RRA180-0.25, RRA180-0.5, RRA180-1, and RRA190-0.5 were 37, 30, 50, 28, 35, 44, and 53 nm, respectively. The PFZ widths increased in the order of RRA180-0.25 < RRA170-2 < RRA180-0.5 < RRA160-4 < RRA180-1 < RRA170-4 < RRA190-0.5. In addition, the continuously distributed GBPs (no interparticle spacing) of T6, RRA160-2, RRA170-1, and RRA180-0.25 were 10–35 nm in length and 3−10 nm in width, while the GBPs of RRA160-4, RRA170-2, RRA180-0.5, and RRA180-1 coarsened to 20−60 nm in length and 3−15 nm in width with an interparticle spacing of 5−60 nm. In contrast, the GBPs of RRA170-4 and RRA190-0.5 further

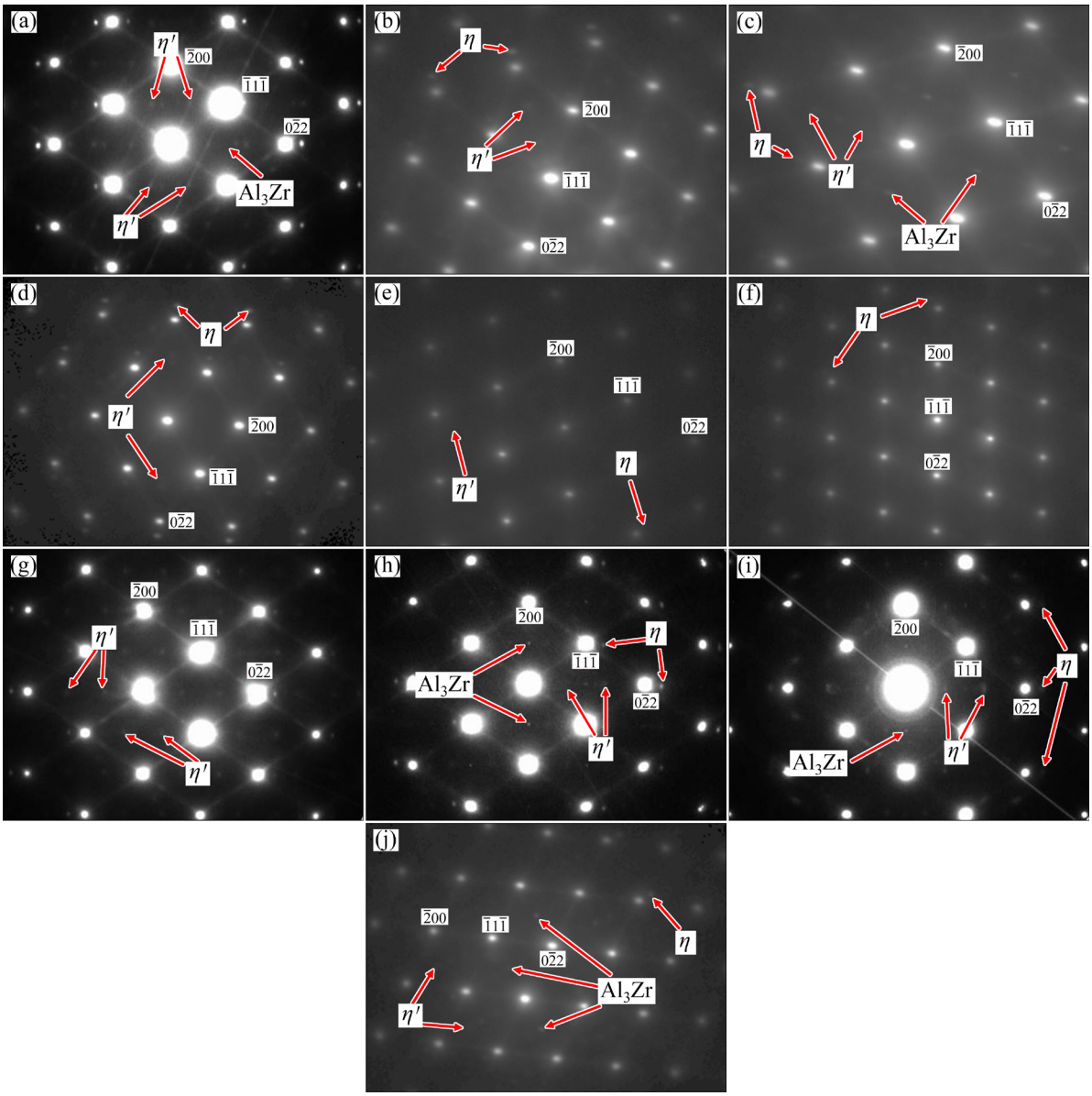

Fig. 7 SAED patterns of 7A85 aluminum alloy after T6 and various RRA treatments: (a) T6; (b) RRA160-2; (c) RRA160-4; (d) RRA170-1; (e) RRA170-2; (f) RRA170-4; (g) RRA180-0.25; (h) RRA180-0.5; (i) RRA180-1; (j) RRA190-0.5

coarsened to 30−85 nm in length and 15−25 nm in width, and their interparticle spacings were 15−70 nm and 100−140 nm, respectively. Increasing the retrogression temperature and time increased the size and interparticle spacing of the GBPs and broadened the PFZ.

3.4 Fracture morphology

The fracture morphologies of 7A85 aluminum alloy after T6 and various aging treatments are shown in Fig. 9. In the T6, RRA180-0.25, and RRA180-0.5 samples, the mixed fracture mode of the intergranular and transgranular fractures and the uniform size distribution of the intergranular fracture dimples were observed. However, large-area intergranular fractures and big dimples occurred in the RR160-2, RRA170-1, and RRA170-2 samples. Upon the increase of the retrogression time, the intergranular fracture ratio decreased accompanied by an increase in the transgranular fracture ratio. Transgranular fracture was prominent in the RRA160-4, RRA170-4, and RRA190-0.5 samples. It can be concluded that the retrogression time had a greater impact on the fracture mechanism of the alloy than the retrogression temperature.

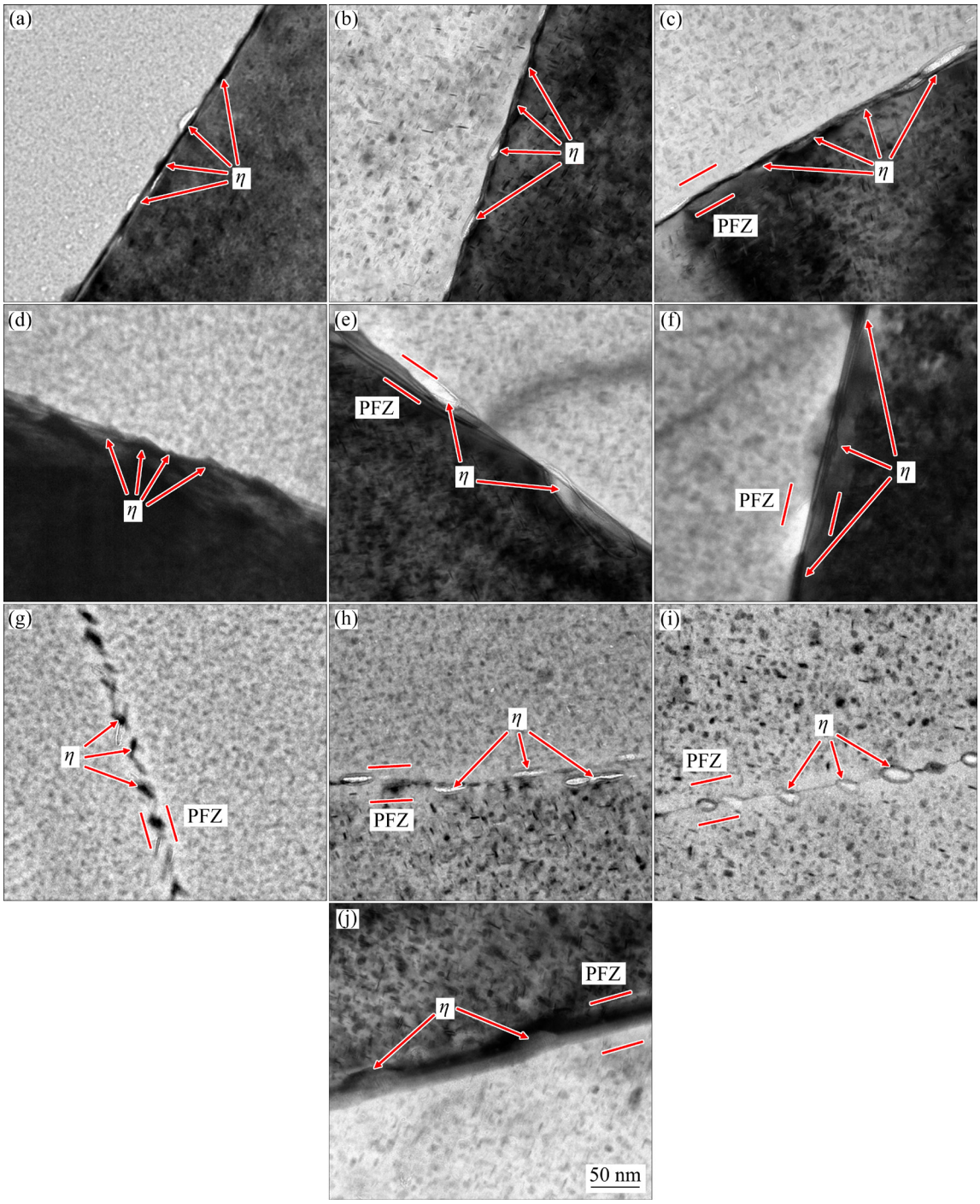

Fig. 8 Grain boundary precipitate morphologies of 7A85 aluminum alloy after T6 and various RRA treatments: (a) T6; (b) RRA160-2; (c) RRA160-4; (d) RRA170-1; (e) RRA170-2; (f) RRA170-4; (g) RRA180-0.25; (h) RRA180-0.5; (i) RRA180-1; (j) RRA190-0.5

4 Discussion

4.1 Precipitation behavior

The above results demonstrate that different RRA treatments have a significant influence on the performance and microstructure of 7A85 aluminum alloy. As a typical age-hardening 7xxx series alloy, the 7A85 aluminum alloy has the following precipitation sequences: supersaturated solid solution (SSS)−coherent GP zones−semi-coherent η'−incoherent stable η [20−22]. The preferential nucleation of the GBPs is caused by the higher energy of the grain boundary than that of the matrix,

which leads to the GBPs being dominated by the state η phases when many GP zones and η' phases precipitate in the matrix. Figure 10 illustrates the evolution of the matrix precipitates and GBPs during RRA aging treatment. In the pre-aging stage, small GP zones and η' phases were formed in the matrix, while continuously distributed η phases with no PFZ were developed at the grain boundaries. The precipitate characteristics at this stage were consistent with that at the T6 state. At high temperatures in the retrogression stage, the GP zones and part of the small-size η' phases in the

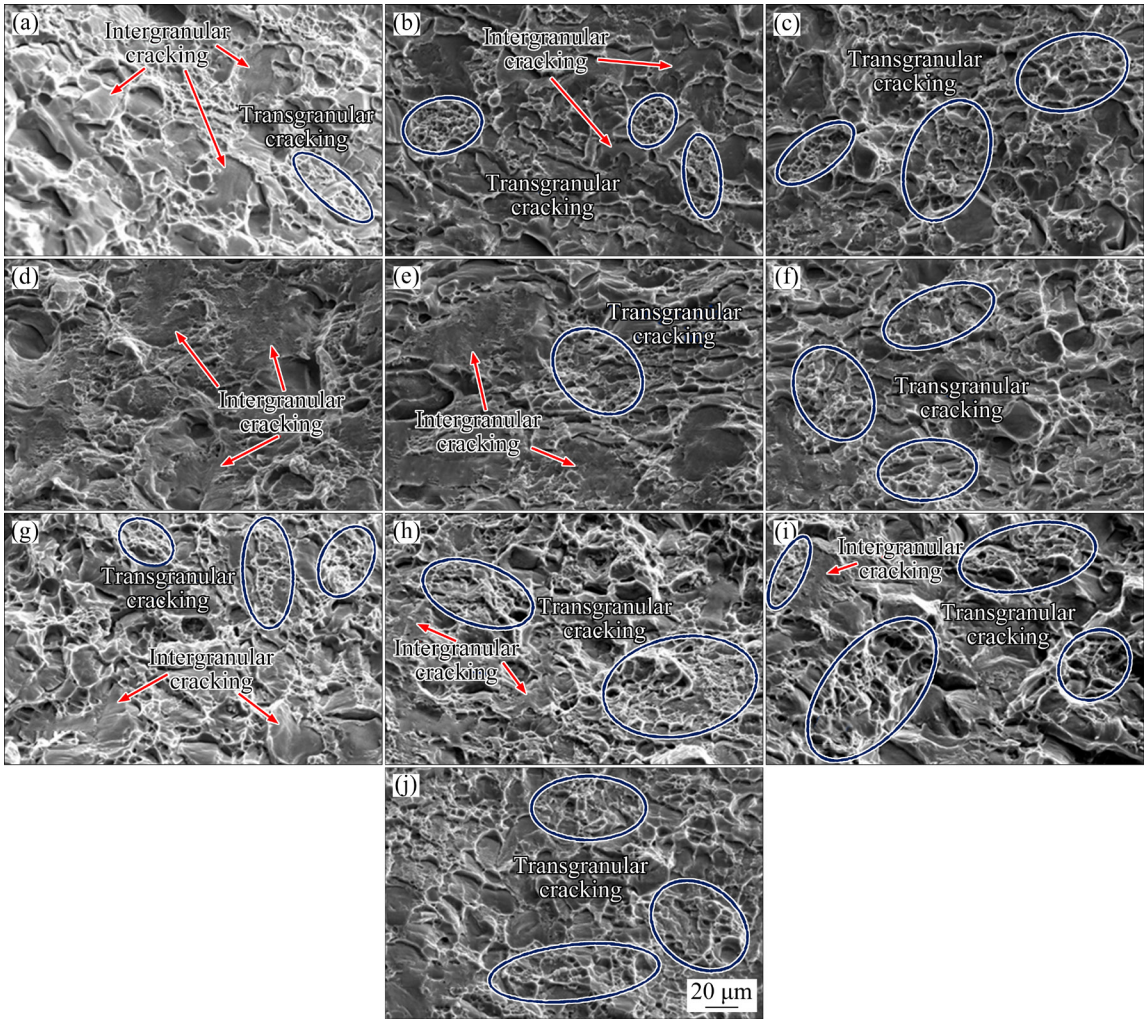

Fig. 9 Fracture morphologies of 7A85 aluminum alloy after T6 and various RRA treatments: (a) T6; (b) RRA160-2; (c) RRA160-4; (d) RRA170-1; (e) RRA170-2; (f) RRA170-4; (g) RRA180-0.25; (h) RRA180-0.5; (i) RRA180-1; (j) RRA190-0.5

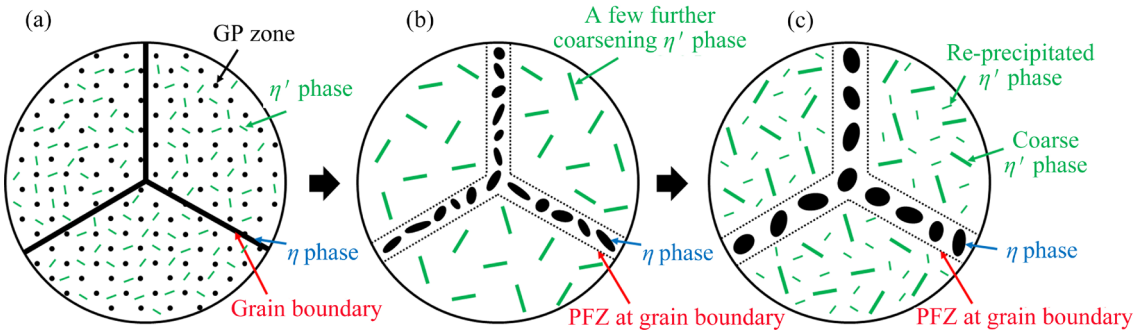

Fig. 10 Precipitate evolution during RRA aging treatment: (a) Pre-aging; (b) Retrogression; (c) Re-aging

matrix dissolved and certain large-size matrix η' phases and coarse η phases at the grain boundaries coarsened. Meanwhile, the matrix precipitate spacing increased and the GBPs with PFZs gradually disconnected. In the re-aging stage, the GP zones and η' phases that dissolved during the retrogression stage re-precipitated in the matrix, and the GBPs continued to coarsen and intermittently distribute. Finally, η' and η phases in the matrix and coarse discontinuously distributed GBPs with wider PFZs were formed after RRA treatment.

4.2 Effect of RRA treatment on mechanical properties and electrical conductivity

4.2.1 Strength

The matrix precipitates can hinder the movement of the dislocations generated during tensile tests. Therefore, the strength of 7A85 aluminum alloy mainly depends on the composition, size and distribution of the matrix precipitates [23,24]. The hindering mechanisms of the precipitates on dislocation movement mainly involve the cutting mechanism and the Orowan bypassing mechanism [25−28]. Under RRA treatment with shorter retrogression time at lower temperatures and T6 tempers, more dislocations are cut by a higher proportion of the fine dispersed η' phases of the matrix, resulting in their hindered movements and the higher strength of the alloy. However, under the RRA tempers with longer retrogression time at higher temperatures, the matrix η' phases coarsened into η phases during the retrogression process, causing an increase in the proportion of coarse η phases in the matrix. The strengthening mechanism in this case is mainly an Orowan bypassing mechanism, as the lower critical shear stress required for dislocations to bypass precipitates is lower than that needed to cut through. The easier dislocation movement results in a reduction in strength.

Similarly, the lower strength of the RRA treatment compared to T6 is due to the growth of some η' phases into η phases during retrogression and re-aging, which eventually produces more matrix η phases with a weaker cutting strengthening. Nevertheless, the strength of RRA180-0.25 exceeds that of T6, as secondary nucleation and secondary precipitation generate a more uniform matrix precipitate distribution and avoid the formation of a few oversized precipitates in the primary precipitation of T6. Moreover, the intermittent distribution of the GBPs with the PFZs of RRA prevents stress concentration at the grain boundaries and the stress relaxation during tensile tests. This results in the significant improvement of the YS for RRA at a suitable retrogression temperature and time compared to T6.

4.2.2 Ductility

Grain boundaries often tend to be weak positions that induce fractures. Thus, the ductility of the alloy is determined by a combination of the matrix and grain boundary characteristics [29,30]. The T6 sample exhibited an extremely high EL compared to the RRA samples as a large number of fine GP zones and η' phases in the matrix allow the stress to be evenly distributed inside the alloy during tensile tests, resulting in the alloy being able to withstand a greater deformation before fracture. At the same retrogression temperature, the EL almost always first decreases and then increases upon extending the retrogression time. Fine matrix precipitates and GBPs with almost no PFZ at short retrogression time produce high matrix and grain boundary strengths with a small strength difference between them, exhibiting a high EL. This is also why the EL of RRA160 is higher than that of RRA170 at a retrogression time below 4 h. Extending the retrogression time to a certain extent leads to the generation of coarser GBPs and PFZ, which reduces the GBP strength and increases the strength difference between the matrix and grain boundaries. The weak grain boundaries induce the premature fracture of the material. Upon further prolonging the retrogression time, the coarsening of the matrix precipitates reduces the strength difference between the matrix and grain boundaries, again improving the EL.

In addition, the RRA-180 and RRA-190 specimens are more likely to obtain higher ELs than the RRA-160 or RRA-170 specimens, since higher retrogression temperatures increase the coarsening rate of the matrix precipitates. Although this greatly reduces the UTS and YS, it also reduces the strength difference between the matrix and grain boundaries, thus significantly improving the EL. Besides, fracture morphology can characterize the EL to a certain extent. The mixed fracture mode of the transgranular and intergranular fractures in the T6 and RRA180-0.25 samples is caused by the small strength difference between the matrix and

grain boundaries which results in random fracture positions and high ELs. The large-area intergranular fractures of RRA160-2 and RRA170-1 are attributed to the weak grain boundary strength, corresponding to low ELs.

4.2.3 Electrical conductivity

For 7xxx series aluminum alloys, high electrical conductivity usually indicates good corrosion properties [17]. The electrical conductivity of alloys is closely related to lattice distortion, matrix precipitates, GBPs, and PFZ at the grain boundaries [10,31]. Many studies have shown that the high content of dissolved atoms within the alloy after solid solution quenching leads to the high lattice distortion. The lattice potential field is destroyed and carriers are easily scattered, resulting in low conductivities after solid solution quenching. During the initial aging stage, although the precipitates that gradually replace dissolved atoms also produce the lattice distortion, they cause less damage to the lattice potential field than dissolved atoms. There is therefore a tendency for the conductivity to increase as the dissolved atoms decrease. In the late aging stage, the lattice distortion produced by the precipitates becomes significant and its barrier to carriers cannot be ignored. This causes differences in the final conductivities for different aging tempers.

MA et al [32] investigated the relationship between the precipitates and conductivity of an Al−Zn−Mg−Cu−Sc−Zr−Ti alloy during aging treatment. The stress field generated by the coherent GP region at the initial stage of precipitation was found to impede electron movement and reduce the conductivity of the alloy. As aging progressed, the formation of the semi-coherent η' phases weakened the electron scattering, thus increasing the conductivity. Subsequently, the non-coherent η phases, which replaced the η' phases, led to more ordered atomic arrangement, lower lattice distortion, and higher conductivity. It was also concluded that the volume fraction of η phases was positively correlated with the electrical conductivity of the alloy. WANG et al [33] determined that the aging temperature of T6 was not high enough to affect the grain boundary structure, thus the effect of GBPs and PFZs on conductivity under T6 could be ignored. Under RRA, the disconnection of GBPs and the formation of PFZs led to a gradual increase in conductivity as the retrogression temperature increased. The conductivity was increased by PFZs due to their establishment of pathways containing a small amount of dissolved atoms, lowering the carrier barriers.

In the present study, for T6, the severe lattice distortions generated by the coherent GP zones and semi-coherent η' phases in the matrix and the continuously distributed GBPs increase the electron diffraction probability, leading to lower conductivity under T6. However, the electrical conductivities following RRA treatment were significantly improved due to the formation of more matrix incoherent η phases and intermittently distributed GBPs with the wide PFZs. High conductivity was more easily obtained at higher retrogression temperatures and longer retrogression time, which was because the increased interparticle spacings of matrix precipitates and GBPs and the wide PFZs at grain boundaries further reduced the electron diffraction. In addition, during the initial stage of retrogression, the conductivity growth rate was greater at the retrogression temperature of 180−190 °C than that at 160−170 °C, indicating a greater influence of the retrogression temperature on conductivities compared to the retrogression time.

4.3 Effect of RRA treatment on corrosion performance

Currently, anodic dissolution has become the prevailing corrosion mechanism for 7xxx series aluminum alloys [34]. The GBPs ($MgZn_2$) have a lower potential than the aluminum matrix, and micro-corrosion cells are easily formed between them, reducing the corrosion performance of the alloy. The continuously distributed GBPs form the anodic corrosion channels that result in the low corrosion resistance of T6, which is significantly improved by the RRA treatment owing to the coarsening and separation of the GBPs during the retrogression and re-aging processes. In agreement with WANG et al [13], increasing the retrogression temperature and time within a certain range enhanced the corrosion resistance of the alloy. This is because the increased interparticle spacing of the GBPs blocks the corrosion channels and reduces the corrosion current density at the grain boundaries. However, the corrosion resistance is deteriorated at excessively high retrogression temperatures and time (RRA170-4 and RRA190-0.5), which can be

related to the PFZ at the grain boundaries. Anodic dissolution exists in two modes: GBP dissolution and PFZ dissolution [35]. The corrosion potential of the η phase at the grain boundaries is lower than that of the PFZ. Thus, the GBPs form micro-corrosion cells with the aluminum matrix, and the PFZ dissolution mechanism is usually inactive. However, it is found that when the width of the PFZs exceeds a certain critical value, the PFZs manifest cathodic characteristics to form micro-corrosion cells with GBPs [36]. Hence, the poor corrosion resistance of RRA170-4 and RRA190-0.5 is attributed to their overly wide PFZs at the grain boundaries (Figs. 8(f) and (j)).

5 Conclusions

(1) Under the RRA with lower retrogression temperature and time and T6 tempers, the finely dispersed matrix precipitates led to the high strength of the alloy, but the continuously distributed GBPs tended to become anodic corrosion channels, resulting in poor corrosion resistance (intergranular and exfoliation corrosion). Upon increasing the retrogression temperature and time, the coarsening of matrix precipitates caused a decrease in the strength of the alloy, while the increased matrix incoherent η phases and the disconnection of GBPs significantly improved its electrical conductivity and corrosion resistance. However, excessively increasing the retrogression temperature and time produced overly wide PFZs, which formed the micro-corrosion cells with the GBPs and reduced the corrosion resistance.

(2) At the same retrogression temperature, the EL first decreased and then increased with the extension of retrogression time, which was due to the small strength difference between the matrix and grain boundaries for both short and long retrogression time. A high EL was easier to obtain at a retrogression temperature of 180 °C, while a lower retrogression time at this temperature could result in the strength exceeding that of the T6 sample.

(3) To optimize the mechanical properties, electrical conductivity, and corrosion resistance of the alloy, the RRA180-0.5 ((120 °C, 24 h) + (180 °C, 0.5 h) + (120 °C, 24 h)) temper was matched to the three-dimensional cryogenically deformed 7A85 aluminum alloy, providing almost no loss of UTS, a 10.1% increase in YS, an 11.9% increase in electrical conductivity, and a 56% decrease in maximum IGC depth compared to T6.

CRediT authorship contribution statement

Dang WANG: Investigation, Methodology, Writing − Original draft; **Wen-xue ZHANG:** Validation, formal analysis, Visualization; **You-ping YI:** Data acquisition, Writing − Review & editing, Funding acquisition; **Shi-quan HUANG:** Resources, Writing − Review & editing, Supervision, Data curation; **Hai-lin HE:** Writing − Review & editing, Software, Data curation; **Jing-jing ZHANG:** Software, Experiments.

Declaration of competing interest

The authors declare that they have no known competing financial interests or personal relationships that could have appeared to influence the work reported in this paper.

Acknowledgments

This work was supported by the National Natural Science Foundation of China (No. 51875583) and the General Program of Natural Science Foundation of Hunan Province, China (No. 2020JJ4709). The authors would like to acknowledge Southwest Aluminum (group) Company Ltd. for its support.

References

[1] CHUNG T F, YANG Y L, SHIOJIRI M, HSIAO C N, LI W C, TSAO C S, SHI Z S, LIN J G, YANG J R. An atomic scale structural investigation of nanometre-sized η precipitates in the 7050 aluminium alloy [J]. Acta Materialia, 2019, 174: 351−368.

[2] XIE Peng, CHEN Song-yi, CHEN Kang-hua, JIAO Hui-bin, HUANG Lan-ping, ZHANG Zhuo, YANG Zhen. Enhancing the stress corrosion cracking resistance of a low-Cu containing Al−Zn−Mg−Cu aluminum alloy by step-quench and aging heat treatment [J]. Corrosion Science, 2019, 161: 108184.

[3] WANG Yi-chang, WU Xiao-dong, YUE Lu, GUO Ming-xing, CAO Ling-fei. Aging precipitation behavior and properties of Al−Zn−Mg−Cu−Zr−Er alloy at different quenching rates [J]. Transactions of Nonferrous Metals Society of China, 2022, 32(4): 1070−1082.

[4] LIU S D, CHEN B, LI C B, DAI Y, DENG Y L, ZHANG X M. Mechanism of low exfoliation corrosion resistance due to slow quenching in high strength aluminium alloy [J]. Corrosion Science, 2015, 91: 203−212.

[5] HOU Yu-zhu, CHEN Liang, LI Zhi-gang, ZHAO Guo-qun, ZHANG Cun-sheng. Effects of artificial aging on microstructure, mechanical properties and stress corrosion

cracking of a novel high strength 7A99 Al alloy [J]. Materials Science and Engineering A, 2020, 780: 139217.

[6] WANG Dang, HUANG Shi-quan, YI You-ping, HE Hai-lin, LI Chen. Effects of cryogenic deformation on the microstructure and mechanical properties of high-strength aluminum alloys [J]. Materials Characterization, 2022, 187: 111831.

[7] ZHANG Ping, LI Yuan-yuan, LIU Ya-nan, ZHANG Ying, LIU Ji-xin. Analysis of the microhardness, mechanical properties and electrical conductivity of 7055 aluminum alloy [J]. Vacuum, 2020, 171: 109005.

[8] REDA Y, YEHIA H M, EL-SHAMY A M. Microstructural and mechanical properties of Al−Zn alloy 7075 during RRA and triple aging [J]. Egyptian Journal of Petroleum, 2022, 31: 9−13.

[9] ANGAPPAN M, SAMPATH V, ASHOK B, DEEPKUMAR V P. Retrogression and re-aging treatment on short transverse tensile properties of 7010 aluminium alloy extrusions [J]. Materials & Design, 2011, 32: 4050−4053.

[10] LI Hui-yan, JIA Li-na, HUANG Jiang-nan, MA Yue. Precipitation behavior and properties of extruded 7136 aluminum alloy under different aging treatments [J]. Chinese Journal of Aeronautics, 2021, 34(2): 612−619.

[11] WANG Qing, ZHAN Li-hua, XU Yong-qian, LIU Chun-hui, ZHAO Xing, XU Ling-zhi, YANG You-liang, CAI Yi-xian. Creep aging behavior of retrogression and re-aged 7150 aluminum alloy [J]. Transactions of Nonferrous Metals Society of China, 2020, 30(10): 2599−2612.

[12] ZHONG Hui-long, LI Sheng-ci, WU Jia-li, DENG Hong-ling, CHEN Ji-qiang, YAN Na, CHEN Zi-xin, DUAN Liang-bo. Effects of retrogression and re-aging treatment on precipitation behavior, mechanical and corrosion properties of a Zr+Er modified Al−Zn−Mg−Cu alloy [J]. Materials Characterization, 2022, 183: 111617.

[13] WANG Yi-chang, CAO Ling-fei, WU Xiao-dong, TONG Xin, LIAO Bin, HUANG Guang-jie, WANG Zhen-gan. Effect of retrogression treatments on microstructure, hardness and corrosion behaviors of aluminum alloy 7085 [J]. Journal of Alloys and Compounds, 2020, 814: 152264.

[14] LI J F, BIRBILIS N, LI C X, JIA Z Q, CAI B, ZHENG Z Q. Influence of retrogression temperature and time on the mechanical properties and exfoliation corrosion behavior of aluminium alloy AA7150 [J]. Materials Characterization, 2009, 60: 1334−1341.

[15] OZER G, KARAASLAN A. Properties of AA7075 aluminum alloy in aging and retrogression and reaging process [J]. Transactions of Nonferrous Metals Society of China, 2017, 27(11): 2357−2362.

[16] WANG Dang, YI You-ping, LI Chen, HUANG Shi-quan, HE Hai-lin, ZHANG Jing-jing. Effects of different multidirectional forging processes on the microstructure and three-dimensional mechanical properties of ultra-high strength aluminum alloys [J]. Materials Science and Engineering A, 2021, 826: 141932.

[17] CHEN Song-yi, CHEN Kang-hua, DONG Peng-xuan, YE Sheng-ping, HUANG Lan-ping. Effect of heat treatment on stress corrosion cracking, fracture toughness and strength of 7085 aluminum alloy [J]. Transactions of Nonferrous Metals Society of China, 2014, 24(7): 2320−2325.

[18] DESCHAMPS A, BRECHET Y. Influence of quench and heating rates on the ageing response of an Al−Zn−Mg−(Zr) alloy [J]. Materials Science and Engineering A, 1998, 251: 200−207.

[19] PARK J K, ARDELL A J. Microstructures of the commercial 7075 Al alloy in the T651 and T7 tempers [J]. Metallurgical and Materials Transactions A, 1983, 14: 1957−1965.

[20] LI Yao, XU Guo-fu, PENG Xiao-yan, LIU Shi-chao, DENG Ying, LIANG Xiao-peng. Effect of non-isothermal aging on microstructure and properties of Al−5.87Zn−2.07Mg−2.42Cu alloys [J]. Transactions of Nonferrous Metals Society of China, 2021, 31(10): 2899−2908.

[21] FANG H C, CHAO H, CHEN K H. Effect of recrystallization on intergranular fracture and corrosion of Al−Zn−Mg−Cu−Zr alloy [J]. Journal of Alloys and Compounds, 2015, 622: 166−173.

[22] LIU Yuan, LIANG Shuai, JIANG Da-ming. Influence of repetitious non-isothermal aging on microstructure and strength of Al−Zn−Mg−Cu alloy [J]. Journal of Alloys and Compounds, 2016, 689: 632−640.

[23] KHAN M A, WANG Y W, AFIFI M A, MALIK A, NAZEER F, YASIN G, BAO J W, ZHANG H. Microstructure and mechanical properties of an Al−Zn−Cu−Mg alloy processed by hot forming processes followed by heat treatments [J]. Materials Characterization, 2019, 157: 109901.

[24] LI Rui-xuan, WILDE G, ZHANG Yong. Synergizing mechanical properties and damping capacities in a lightweight Al−Zn−Li−Mg−Cu alloy [J]. Journal of Alloys and Compounds, 2021, 886: 161285.

[25] ZHANG Zhao-gang, MA Xin-wu, ZHANG Cun-sheng, CHU Guan-nan, MENG Zi-jie, ZHAO Guo-qun, CHEN Liang. Effect of stress-aging treatment on the mechanical and corrosion properties of Al−Zn−Mg−Cu alloy [J]. Materials Science and Engineering A, 2022, 838: 142791.

[26] GALINDO-NAVA E I, RAE C M F. Microstructure-sensitive modelling of dislocation creep in polycrystalline FCC alloys: Orowan theory revisited [J]. Materials Science and Engineering A, 2016, 651: 116−126.

[27] YANG Rong-xian, LIU Zhi-yi, YING Pu-you, LI Jun-lin, LIN Liang-hua, ZENG Su-ming. Multistage-aging process effect on formation of GP zones and mechanical properties in Al−Zn−Mg−Cu alloy [J]. Transactions of Nonferrous Metals Society of China, 2016, 26(5): 1183−1190.

[28] XIAO Quan-feng, HUANG Ji-wu, JIANG Ying-ge, JIANG Fu-qin, WU Yun-feng, XU Guo-fu. Effects of minor Sc and Zr additions on mechanical properties and microstructure evolution of Al−Zn−Mg−Cu alloys [J]. Transactions of Nonferrous Metals Society of China, 2020, 30(6): 1429−1438.

[29] ZHU Hong-xu, MA Pei-pei, LIU Chun-hui, HE Jun, YANG Jian-shi, CHEN Long-hui, HUANG Lan-ping, ZHAN Li-hua. Effect of cryogenic pre-deformation on the stress relaxation response and mechanical/corrosion properties in Al−Zn−Mg−Cu alloy [J]. Journal of Materials Research and Technology, 2022, 20: 3471−3484.

[30] LIU Tao, JIANG Hai-tao, SUN Hui, WANG Yu-jie, DONG Qing, ZENG Jian-rong, BIAN Feng-gang, ZHANG Jiao,

CHEN Fei, SUN Bao-de. Effects of rolling deformation on precipitation behavior and mechanical properties of Al−Zn−Mg−Cu alloy [J]. Materials Science and Engineering A, 2022, 847: 143342.

[31] HOU L G, YU H, WANG Y W, YOU L, HE Z B, WU C M, ESKIN D G, KATGERMAN L, ZHUANG L Z, ZHANG J S. Tailoring precipitation/properties and related mechanisms for a high-strength aluminum alloy plate via low-temperature retrogression and re-aging processes [J]. Journal of Materials Science & Technology, 2022, 120: 15−35.

[32] MA Yun-long, HUANG Yuan-chun, ZHANG Xie-yi. Precipitation thermodynamics and kinetics of the second phase of Al−Zn−Mg−Cu−Sc−Zr−Ti aluminum alloy [J]. Journal of Materials Research and Technology, 2021, 10: 445−452.

[33] WANG Ying-chen, LIU Mao-wen, XIAO Wen-long, ZHAO Wei-tao, MA Chao-li. Effects of multi-stage aging treatments on the precipitation behavior and properties of 7136 aluminum alloy [J]. Journal of Alloys and Compounds, 2020, 814: 152256.

[34] PENG Xiao-yan, GUO Qi, LIANG Xiao-peng, DENG Ying, GU Yi, XU Guo-fu, YIN Zhi-min. Mechanical properties, corrosion behavior and microstructures of a non-isothermal ageing treated Al−Zn−Mg−Cu alloy [J]. Materials Science and Engineering A, 2017, 688: 146−154.

[35] ROMHANJI E, POPOVIĆ M. Problems and prospect of Al−Mg alloys application in marine constructions [J]. Metalurgija, 2006, 12: 297−307.

[36] SONG Feng-xuan, ZHANG Xin-ming, LIU Sheng-dan, TAN Qi, LI Dong-feng. The effect of quench rate and overageing temper on the corrosion behaviour of AA7050 [J]. Corrosion Science, 2014, 78: 276−286.

回归温度和时间对深冷变形 7A85 铝合金显微组织、力学性能和腐蚀行为的影响

王 当[1,2]，张文学[1,3]，易幼平[1,2,4]，黄始全[1,2,4]，何海林[1,2]，张京京[2,4]

1. 中南大学 轻合金研究院，长沙 410083；
2. 中南大学 高性能复杂制造国家重点实验室，长沙 410083；
3. 首都航天机械有限公司，北京 100076；
4. 中南大学 机电工程学院，长沙 410083

摘 要：为了平衡合金的强度、塑性与耐蚀性，在不同回归温度和时间条件下对深冷变形 7A85 铝合金的显微组织和综合性能进行研究。结果表明，在较低回归温度和时间的回归再时效(RRA)制度和 T6 (120 ℃, 24 h)制度下，合金具有较高的强度，但耐蚀性较差。对于 RRA，在一定范围内增加回归温度和时间会降低合金的强度，但合金的电导率和耐蚀性显著提高。然而，过度地增加回归温度和时间使合金的耐蚀性降低。相同的回归温度下，随着回归时间的延长，合金的伸长率先减小后增大。与三向深冷变形 7A85 铝合金的最佳匹配的制度为 RRA180-0.5 ((120 ℃, 24 h) + (180 ℃, 0.5 h) + (120 ℃, 24 h))。

关键词：深冷变形 7A85 铝合金；回归温度；回归时间；强度；耐蚀性；最佳制度

(Edited by Wei-ping CHEN)